Rubrene Untwisted: Common Density Functional Theory Calculations Overestimate Its Deviant Tendencies

Journal:	*Journal of Materials Chemistry C*
Manuscript ID	TC-ART-11-2020-005463.R2
Article Type:	Paper
Date Submitted by the Author:	26-Jan-2021
Complete List of Authors:	Greenwell, Chandler; University of California Riverside, Chemistry Beran, Gregory; University of California Riverside, Chemistry

Journal Name

Rubrene Untwisted: Common Density Functional Theory Calculations Overestimate Its Deviant Tendencies[†]

Chandler Greenwell[a] and Gregory J. O. Beran[*a]

The exceptionally high carrier mobility of rubrene derives from the combination of its intrinsic electronic properties and favorable crystal packing that facilitates charge transport. Unlike the planar conformations adopted by rubrene single crystals, however, many rubrene derivatives crystallize with a twisted tetracene core and exhibit poor carrier mobility. Typical density functional theory (DFT) calculations suggest that the twisted conformation is preferred by ∼10–14 kJ/mol or more in the gas phase. However, the present work shows that those calculations overestimate the twisting energy by several kJ/mol due to density-driven delocalization error, and that the twisting energies are actually only ∼8–10 kJ/mol for typical rubrene derivatives when computed with higher-level correlated wave function models. This result has two significant implications for crystal engineering with rubrene derivatives: First, DFT calculations can erroneously predict polymorphs containing twisted rubrene conformations to be more stable, when in fact structures with planar conformations are preferred, as is demonstrated here for perfluororubrene. Second, the smaller twisting energies make it more likely that solid form screening could discover new planar-core polymorphs of rubrene derivatives that have previously been crystallized only in a twisted conformation. These in turn might exhibit better organic semiconducting properties.

1 Introduction

High carrier mobility of 20–40 cm^2/Vs[1] makes rubrene stand out among organic semiconductors, along with high-carrier-mobility derivatives of benzothienobenzothiophene (BTBT), dinaphthothienothiophene (DNTT), and dibenzothiophenothienothiophene (DBTTT).[2] However, the rubrene carrier mobility drops precipitously in solution or thin film devices due to a change in the intramolecular conformation from a planar tetracene backbone in the solid-state to a twisted backbone structure in the other phases (Figure 1).[3] The unique semiconducting properties in crystalline rubrene result from favorable overlap between rubrene molecules with planar tetracene backbones and favorable intermolecular interactions with neighboring molecules.[4,5] Twisting of the tetracene backbone and the concomitant changes in crystal packing disrupt both of these favorable interactions.

For many years, researchers have probed the chemical space of rubrene derivatives and other oligoacenes in pursuit of a superior organic semiconductor. Although many interesting materials have emerged from this research,[2,6] none has yet matched rubrene's superior charge mobility. High carrier mobility in rubrene deriva-
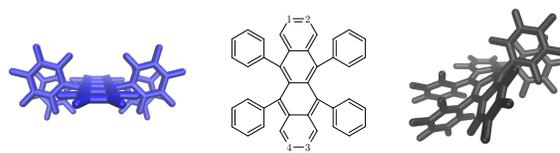
Fig. 1 Rubrene in its planar (blue) and 60° twisted (gray) conformations. The twisting is defined by the dihedral angle formed from atoms 1–4.

tives is frequently associated with the molecule having a planar tetracene core and favorable intermolecular packing.[7–11] While all three known crystal polymorphs of rubrene exhibit planar tetracene backbones,[12,13] other rubrene derivatives can adopt either planar or twisted conformations in the solid-state.[6–11,14–19] The solid-state conformation adopted by a given derivative is difficult to predict *a priori* from chemical intuition alone, although the electron donating and withdrawing properties of functional groups are loosely correlated with twisted or planar structures respectively[10]. In some cases, a given derivative can form both planar and twisted crystal polymorphs.[8,20,21] Extensive analysis of the intramolecular conformational energies and intermolecular packing interactions found that symmetric intermolecular interactions are needed in the crystal to stabilize the planar tetracene backbone.[11] This same study highlights how when chemically modifying rubrene, one must consider both the opportunity to

[a] Department of Chemistry, University of California Riverside, Riverside CA 92521, USA
Tel: +1 951-827-7869; E-mail: gregory.beran@ucr.edu

form new interactions and the potential for disrupting existing favorable interactions.

The complex interplay of intra- and intermolecular interactions makes crystal engineering particularly challenging for conformationally flexible molecules like rubrene, especially since the energy differences between experimentally observed crystal polymorphs are typically within 10 kJ/mol and are often much smaller[22–24]—i.e. no more than a few times kT at room temperature. Crystal structure prediction seeks to predict the entire crystal energy landscape—the set of all energetically favorable crystal structures.[25,26] From this landscape, it is ideally possible to identify both the most stable crystal packing motifs and perhaps other low-energy crystal forms with desired properties. Crystal structure prediction has grown increasingly reliable in recent years, as evidenced by successes in recent blind tests[27–29] and other applications.[30–36] A number of pharmaceutical companies now incorporate it into the solid form screening stages of drug development.[26,37] This raises the prospects of using crystal structure prediction to search for crystal structures of rubrene derivatives which exhibit good intramolecular structural and electronic properties as well as suitable intermolecular packing. Crystal structure prediction has already been used to design new highly porous organic materials[31] and to screen organic semi-conductor materials.[38–40]

However, *in silico* design strategies are effective only if the models used correctly predict the stabilities of the crystal structures. Density functional theory (DFT) is widely used for modeling the energetic, structural, and electronic properties of organic materials[41–43] because it generally balances between accuracy and computational efficiency well. The omission of van der Waals dispersion interactions from widely used generalized gradient approximation (GGA) and hybrid density functionals was previously a problem, but this limitation has been overcome through the development of good-quality dispersion corrections.[44,45] On the other hand, delocalization error remains pervasive in these functionals[46,47] and can lead to surprisingly large problems in organic materials. For example, delocalization error can cause spurious proton transfer which artificially converts a neutral multi-component crystal into its salt form.[48] It leads to underestimation of barrier heights[49–52] and dissociation energies.[53–55] Delocalization error can artificially stabilize molecules with more extended π conjugation relative to those with less.[56–58] A number of organic and pharmaceutical conformational polymorphs have been found where delocalization error and the competition between highly conjugated planar conformations and less-conjugated non-planar conformations leads to incorrect polymorph stabilities.[59,60]

Delocalization error can often be attributed to errors in the electron density.[61] In such cases, improving the electron density can improve the energetics for a given density functional considerably.[62–65] However, obtaining quantitatively accurate results may require using more advanced density functionals (e.g. double-hybrid functionals) or wave function-based models. Unfortunately, such models are often too computationally demanding for direct application to solid-state organic materials. We have recently demonstrated that dispersion-corrected second-

order Møller-Plesset perturbation theory (MP2D)[66] and its spin-component-scaled analog SCS-MP2D[67] can predict conformational energies far more accurately than typical GGA and hybrid density functionals. These models build on a long history of applying spin-component scaling[68–76] and dispersion correction[77–81] to MP2 to achieve a well-balanced model that is competitive with many top-tier double-hybrid and range-separated density functionals in terms of accuracy and computational cost.[67] Combining intramolecular MP2D (to describe the conformational energy) with intermolecular DFT (to describe the lattice contributions) leads to greatly improved polymorph stabilities in a number of conformational polymorphs ranging from small molecules like ortho-acetamidobenzamide[60] to pharmaceuticals like galunisertib and axitinib[60] and photomechanical materials like 9-tert-butyl anthracene ester.[82]

The present study revisits the energetics associated with planar and twisted rubrene conformations with high-quality electronic structure methods. We demonstrate how commonly used density functionals artificially stabilize the twisted form of rubrene relative to the planar one by several kJ/mol, which represents a chemically important fraction of the twisting energy. More significantly, we show how these poor conformational energy differences can artificially bias predictions of crystal stability toward polymorphs containing twisted rubrene molecules instead of planar ones. This means that naive DFT modeling of these crystals can produce misleading results regarding the thermodynamic stability of polymorphs for rubrene-like molecules that differ in the conformations of their tetracene cores. Moreover, in contrast to many earlier DFT estimates,[10,11,21,83] the smaller conformational energy differences between twisted and planar rubrenes found here lie well within the typical energy window associated with conformational polymorphism.[22,23,84] This suggests that conformational polymorphs are more likely to occur than previous results would have indicated. Therefore, it could be worthwhile screening more extensively for planar-backbone polymorphs of rubrene derivatives which are known to crystallize in a twisted conformation, since data on existing derivatives indicates that planar polymorphs are more likely to exhibit high carrier mobility.

2   Computational Methods

To investigate the twisting energies of rubrene and its derivatives, gas-phase structures were optimized at the B3LYP/cc-pVDZ level of theory using Gaussian 09.[85] Although this functional omits description of van der Waals dispersion, it was chosen to match earlier work.[10] These optimizations include a series of constrained optimizations with tetracene backbone twists ranging from 0–60° to map out the twisting energy curves for rubrene, half-fluorinated rubrene (F_{14}-rubrene), and perfluororubrene. For the rubrene derivatives taken from ref 10, twisted structures were obtained via complete relaxation of the structures, while planar ones were obtained via constrained optimization.

Single-point energies were then computed for these structures using a variety of dispersion-inclusive density functionals and correlated wavefunction methods, primarily using PSI4.[86] The DFT functionals employ the def2-QZVP basis.[87] MP2 correlation energies were extrapolated to the complete-basis-set (CBS) limit[88]

from the aug-cc-pVTZ and aug-cc-pVQZ basis sets, [89] and these results were combined with Hartree-Fock (HF)/aug-cc-pVQZ. SCS-MP2D results were obtained from the PSI4 MP2 values and an in-house code which performs the correction. Benchmark domain-based local pair natural orbital coupled cluster singles, doubles, and perturbative triples (DLPNO-CCSD(T)) [90] calculations were performed in the cc-pVTZ basis using ORCA [91] and extrapolated to the CBS limit by combining them with the MP2/CBS results using the standard focal point technique, [92]

$$E_{CBS}^{CCSD(T)} = E_{CBS}^{MP2} + \left(E_{cc-pVTZ}^{CCSD(T)} - E_{cc-pVTZ}^{MP2} \right). \qquad (1)$$

The DLPNO-CCSD(T) calculations employed both tight self-consistent field and pair-natural orbital settings to achieve better fidelity to canonical CCSD(T) results.

Finally crystalline calculations were performed for three polymorphs of rubrene (Cambridge Structure Database reference codes QQQCIG07, [12] QQQCIG13, [13] QQQCIG14 [13]) and two polymorphs of perfluororubrene (INELUK02 and INELUK03 [21]). The structures were fully relaxed with the dispersion-corrected B86bPBE-XDM functional using QuantumEspresso. [93]. A kinetic energy cutoff of 50 Ry was used for the wavefunctions, and a charge density and potential cutoff of 500 Ry was used. Core electrons were treated via the projector augmented wave (PAW) approach using PAW potentials for H, C, and F generated with A. Dal Corso's Atomic code v6.1. Monkhorst-Pack k-point sampling grids were used as specified in Supporting Information (SI) Table S5. The agreement between the optimized and experimental crystal structures is characterized by the rmsd15 metric, [94] which measures the root-mean-square deviation for a cluster of 15 molecules from the crystal (excluding hydrogen atoms). The crystal energies were then refined via the monomer-correction approach, [60] in which the crystal energy is corrected based on the gas-phase molecular conformational energy differences between B86bPBE-XDM and a higher level of theory.

3　Results and Discussion

3.1　Gas-phase twisting energies

We begin by benchmarking the potential energy curves generated by twisting the tetracene backbone dihedral angle from 0-60° for rubrene, its half-fluorinated F_{14}-rubrene derivative, and the completely fluorinated perfluororubrene. Figure 2 compares the potential energy curves generated by PBE-D3(BJ), B86bPBE-XDM, B3LYP-D3(BJ), SCS-MP2D, and DLPNO-CCSD(T). PBE and B3LYP were chosen as representative of widely-used GGA and hybrid density functionals; similar results are also obtained with other common GGA and hybrid functionals as well. The B86bPBE-XDM GGA functional is included in the gas-phase calculations here because it is used in the solid-state calculations in the next section.

Backbone twisting stabilizes all three rubrene systems, though fluorination increases the optimal extent of twisting. More significantly, the energy stabilization achieved by twisting the tetracene backbone varies considerably depending on the computational model used. For example, all five methods shown in Figure 2a predict a minimum near 40° for rubrene. However, whereas the three density functionals predict that the twisted form is about 12

kJ/mol more stable than the planar one, SCS-MP2D and DLPNO-CCSD(T) find the minimum to be closer to 9 kJ/mol.

For perfluororubrene, the SCS-MP2D, and DLPNO-CCSD(T) methods agree that the minimum energy occurs at 50°, whereas the curve continues to decrease with PBE-D3(BJ) and B86bPBE-XDM, and it becomes flat for B3LYP-D3(BJ). Furthermore, SCS-MP2D and DLPNO-CCSD(T) predict the minimum energy to be near 8 kJ/mol. On the other hand, the three density functionals predict the energy to be 4–6 kJ/mol lower. Similar behavior is seen for the half-fluorinated rubrene derivative in Figure 2b, for which the density functionals twist the backbone too much and over-stabilize the twisted form by about 5 kJ/mol.

Taking the DLPNO-CCSD(T) results as benchmark values, the density functionals exhibit root-mean-square errors of 3–4 kJ/mol across these three potential curves, compared to only 0.4 kJ/mol for SCS-MP2D. So while the SCS-MP2D single-point energy calculations are more computationally demanding than the DFT ones, they cost only a small fraction of what the DLPNO-CCSD(T) ones cost.

The same tendency for density functional theory models to over-stabilize the twisted tetracene backbone manifests in other rubrene derivatives. In 2013, McGarry and co-workers synthesized a series of rubrene derivatives with fluoro, methyl, or tri-fluromethyl groups substituted on the phenyl rings. [15] All of these species adopt a gas-phase geometry in which the tetracene backbone twists by ∼30–40°. The PBE-D3(BJ), B86bPBE-XDM, and B3LYP-D3(BJ) density functionals once again over-stabilize the twisted form relative to the planar one for all of these derivatives, with root-mean-square errors (RMSE) of 2.8–2.9 kJ/mol relative to DLPNO-CCSD(T) benchmarks (Table 1). Previous studies have also employed functionals such as ωB97, ωB97X-D, and M06-L for these systems. [10,11] The long-range-corrected hybrid functional ωB97X-V performs considerably better than the other functionals tested and reduces the RMSE to 1.6 kJ/mol (Table 1), while ωB97 and M06-L give larger RMSEs of 2.6 and 4.7 kJ/mol, respectively (Table S2). However, all of the functionals tested here exhibit considerably larger errors than SCS-MP2D, which reproduces the DLPNO-CCSD(T) twisting energies to within an RMSE of 0.2 kJ/mol (and at fraction of the computational cost of coupled cluster theory). MP2D, which corrects the van der Waals dispersion in MP2 but does not employ spin-component scaling, performs similarly to SCS-MP2D, albeit with a slightly larger 0.8 kJ/mol RMSE (Table S2). The next section investigates the origins of these erroneous DFT twisting energies in terms of delocalization error, while Section 3.3 demonstrates how these errors can impact the modeling of rubrene derivatives in the solid state.

3.2　Theoretical origins of the DFT twisting energy errors

The problematic twisting energies observed in Section 3.1 arise from delocalization error in the density functionals. The literature contains numerous examples where delocalization error over-stabilizes planar structures with extended π-conjugation relative to non-planar ones with reduced conjugation, [56,58,59,95] and one might therefore expect semi-local density functionals like those used here to artificially stabilize the planar form relative

Table 1 Energy differences, $\Delta E = E_{twist} - E_{planar}$, between the planar and twisted forms of rubrene and four derivatives (kJ/mol), and the root-mean-square error relative to the benchmark DLPNO-CCSD(T) results.
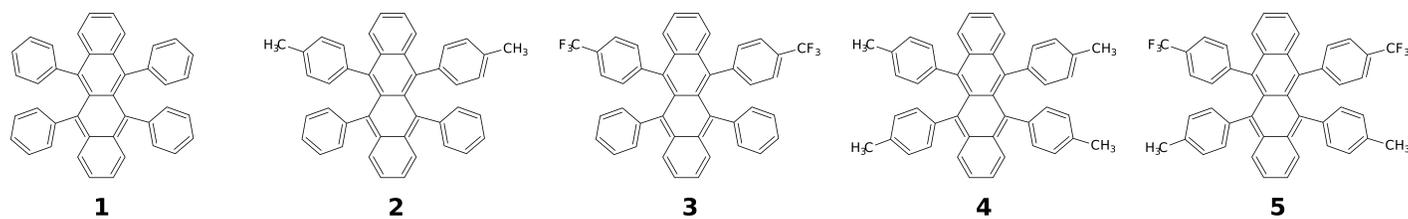
Species	PBE-D3(BJ)	B86bPBE-XDM	B3LYP-D3(BJ)	ωB97X-V	SCS-MP2D	DLPNO-CCSD(T)
1	-12.0	-12.2	-12.1	-10.9	-9.4	-9.3
2	-11.9	-12.1	-11.8	-10.6	-9.1	-9.0
3	-11.2	-11.0	-11.6	-10.7	-8.6	-9.0
4	-11.5	-11.7	-11.2	-10.0	-8.4	-8.4
5	-10.6	-10.6	-10.4	-8.9	-7.5	-7.2
RMSE	2.9	2.9	2.8	1.6	0.2	

to the twisted one. However, the rubrene data above contradicts this assumption—the twisted form is artificially stabilized, not the planar one. Moreover, twisting the tetracene backbone does not significantly disrupt the π conjugation; electronic properties such as frontier orbital energies and Mulliken atomic charges change minimally upon twisting (SI Section S2).

Rubrene twisting is governed by two competing factors: Twisting the tetracene backbone is energetically unfavorable, but it allows the phenyl rings to shift apart and reduce the repulsive exchange interactions between them.[10] The tetracene backbone twisting is the largest single source of error, accounting for about 60% of discrepancy between PBE-D3(BJ) and SCS-MP2D, and it bears the hallmarks of electron density-driven delocalization error.[61] As shown in Figure 3, the tetracene twisting energy varies nearly linearly with the fraction of exact exchange included in the functional. Similar linear variation is observed for the Mulliken atomic charges and frontier orbital energies (SI Figure S1). This behavior also helps explain the somewhat improved performance of the long-range corrected hybrid functional ωB97X-D noted above.

In systems plagued by density-driven delocalization error, correcting the electron density greatly improves the energies obtained from the density functionals. For example, replacing DFT densities with densities derived from the Hartree-Fock orbitals substantially improves the barrier heights, dissociation energies, and potential energy surfaces obtained across a variety of systems.[61–65] Here, the same density substitution considerably improves the rubrene twisting energetics for all three functionals shown in Figure 3. Taken together, this data demonstrates that density-driven delocalization error plays a significant role in the DFT twisting energy errors.

The next section shows how these errors can have a chemically significant impact on the predicted stabilities of rubrene derivatives in the solid state. Unlike these density functionals, correlated wavefunction methods like SCS-MP2D and DLPNO-CCSD(T) are not plagued by these delocalization error effects and can be used to improve the description of the solid state stabilities.

3.3 Impact on solid state polymorph stabilities

Having seen how standard density functionals artificially stabilize the twisted conformation of rubrene and its derivatives, we now examine how this behavior can lead to incorrect predictions of rubrene behavior in the solid state. Perfluororubrene can adopt multiple crystal forms, including a monoclinic polymorph with a planar rubrene backbone conformation and another with a twisted conformation (Figure 4a).[20,21] Although the relative thermodynamic stabilities of these two polymorphs has not been reported experimentally, we can investigate them computationally. After relaxing the experimental crystal structures with the dispersion-corrected GGA functional B86bPBE-XDM, the agreement between the DFT and experimental crystal structures is excellent, with rmsd15 values of 0.08–0.09 Å (Table S5), and the molecular conformations are visually indistinguishable between the optimized and experimental structures. B86bPBE-XDM predicts the twisted polymorph to be 3.5 kJ/mol more stable (Figure 5a). However, this functional is expected to artificially stabilize the twisted polymorph due to the conformational energy errors discussed above, despite the excellent quality of the optimized structures.

Calculating the periodic perfluororubrene crystal energies with state-of-the-art density functionals or correlated wave function methods would be very computationally expensive. However, in cases where the primary deficiency of the DFT functional lies in the intramolecular conformational energy, a monomer-correction approach that replaces the DFT conformational energy with a higher-level one can dramatically improve the polymorph energies.[60] Figure 5a plots the relative polymorph energy differences for the two perfluororubrene polymorphs after correcting the intramolecular conformational energies. Refining the conformational energies with PBE-D3(BJ) or B3LYP-D3(BJ) has little impact on the polymorph energies, since they also over-stabilize the twisted conformation. On the other hand, refining the conformational energies with SCS-MP2D or DLPNO-CCSD(T) completely reverses the polymorph stabilities, shifting the the planar form from being 3.5 kJ/mol less stable than the twisted one to being 3–4 kJ/mol more stable—a ~7–8 kJ/mol correction. MP2D

(a) Rubrene

(b) F_{14}-rubrene
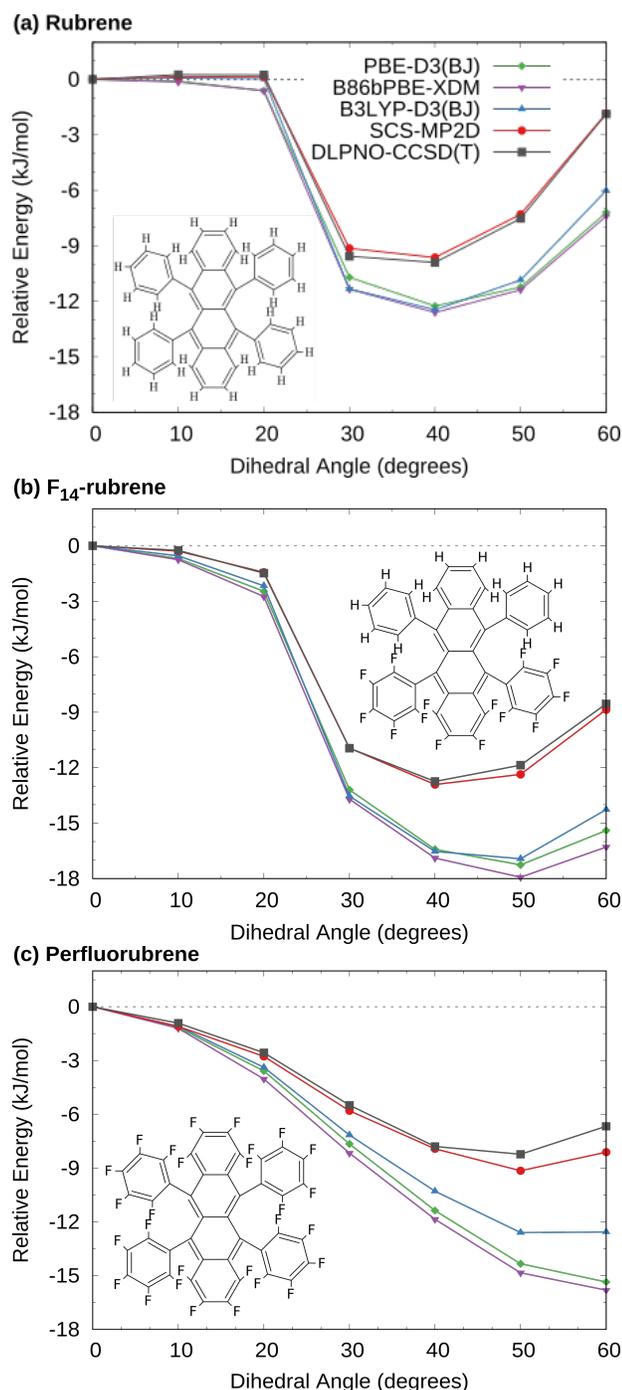
(c) Perfluorubrene

Fig. 2 Potential energy scans for twisting the dihedral angle defined by atoms 1–4 in Figure 1 from 0° to 60° in (a) rubrene, (b) half-fluorinated F_{14}-rubrene, and (c) perfluorubrene.
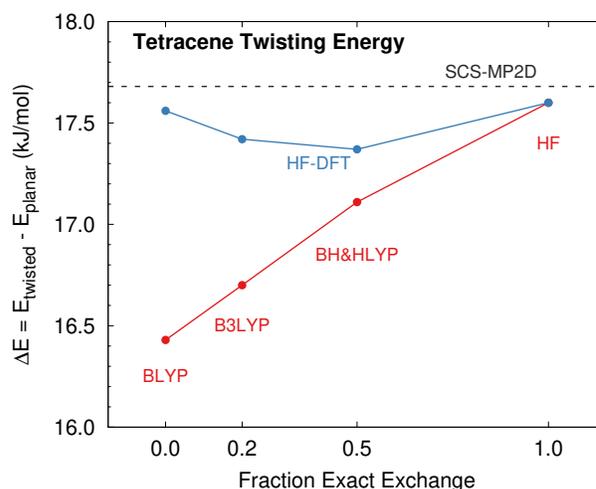
Fig. 3 The twisting energy of the tetracene backbone varies nearly linearly with the fraction of exact exchange included in the functional. Evaluating the energy of the same functionals with HF densities instead of the DFT ones (HF-DFT) dramatically reduces the dependence on the fraction of exact exchange and leads to results in far better agreement with SCS-MP2D.

performs similarly, though in this case it predicts a value in almost perfect agreement with DLPNO-CCSD(T) (Table S3). The range-separated hybrid functional ωB97X-V performs better than the simpler B3LYP or PBE functionals, but it captures only about half the necessary correction and does not fix the incorrect polymorph stability ordering. As shown in SI Section S3, using crystals constrained to the experimental lattice parameters instead of the fully relaxed unit cells used in Figure 5 alters the relative polymorph energies by less than 1 kJ/mol, suggesting that these perfluororubrene energies are not too sensitive to modest changes in the unit cell volumes. Overall, this perfluororubrene example highlights the chemically important impact of these DFT errors— incorrectly predicting the thermodynamically stable crystal form by a substantial margin.

In contrast to the perfluororubrene polymorphs, one expects much better performance for common density functionals with or without monomer-corrections when ranking among a set of polymorphs that exhibit very similar intramolecular conformations. For example, the orthorhombic, monoclinic, and triclinic polymorphs of rubrene all contain planar tetracene backbones (Figure 4b). [12,13] As shown in Figure 5b, the monomer correction alters the B86bPBE-XDM relative energies of the triclinic and monoclinic forms versus the orthorhombic one by less than 2 kJ/mol, compared to the ~7–8 kJ/mol shift seen for the perfluororubrene polymorphs. Any errors made in the planar conformational energy will largely cancel in the relative polymorph energy differences, and the relative DFT stabilities for these three planar polymorphs of rubrene are far more reasonable than they are for comparing the planar and twisted forms of perfluororubrene.

Interestingly, the SCS-MP2D and DLPNO-CCSD(T) monomer-corrected results do suggest that triclinic rubrene is 0.3–0.7 kJ/mol more stable in lattice energy than the commonly crystallized orthorhombic form. Qualitatively similar results are
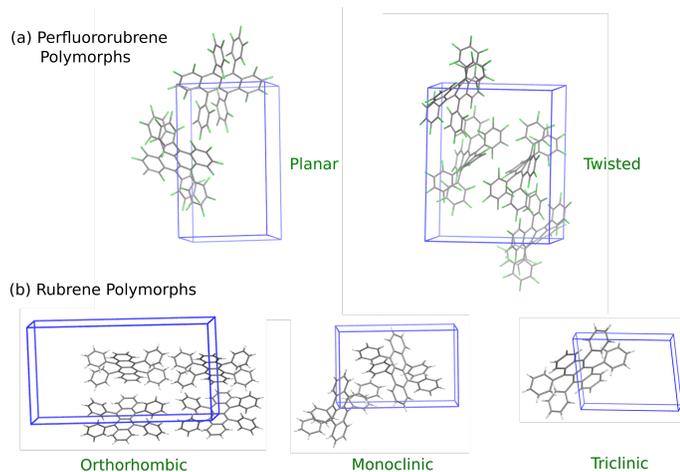
Fig. 4 Crystal structures of the (a) perfluororubrene and (b) rubrene polymorphs studied here. The twisted polymorph of perfluororubrene has a 46° tetracene dihedral angle twist experimentally (and 48.5° in the DFT-relaxed structure). The other four structures have planar backbones (0° dihedral).

found with the hybrid B3LYP-D3(BJ) and range-separated hybrid ωB97X-V density functionals (SI Table S3). This result may seem surprising, since the widely obtained orthorhombic polymorph is probably the thermodynamically stable one experimentally. Of course, these lattice energies neglect the phonon contributions to the free energies at finite temperature, which typically alter polymorph stabilities by 1–2 kJ/mol[24] and can be important for ranking close-lying polymorphs.[34,96–100] Indeed, previous work on rubrene has shown that the zero-point vibrational energy contributions destabilize the monoclinic and triclinic forms relative to the orthorhombic one,[43] and it seems therefore quite possible that including phonon contributions to the free energy would restore the orthorhombic form as the thermodynamically preferred one. Such nuances do complicate crystal structure prediction, but it is important to reiterate that these phonon contributions are typically considerably smaller than the GGA twisting energy problems seen in perfluororubrene.

Finally, the computational cost of the single-point SCS-MP2D monomer correction energy is modest compared to the planewave DFT geometry optimization of the crystal. For example, on an Intel Xeon E5-2680v3, optimizing the monoclinic polymorph of rubrene with two molecules in the unit cell ($Z = 2$) required about 650 central processing unit (CPU) hours, while the single-point monomer correction consumed about a third of that at 220 CPU hours. The cost ratio for the two calculations varies with the crystal structure: the planewave calculation cost is governed primarily by the size of the unit cell, while the gas-phase monomer correction cost scales with the size of the isolated molecule and the number of symmetrically unique molecules in the unit cell. Therefore, the monomer-correction represents a considerably smaller fraction of the CPU time for the orthorhombic polymorph ($Z = 4$), and a larger one for the triclinic polymorph ($Z = 1$). Overall, the monomer correction can be computed readily for species containing $\sim$100 atoms, and it can readily be applied to many structures on the crystal energy landscape.[60]

4 Conclusions

Overall, these results highlight how standard GGA and hybrid density functionals over-stabilize twisted forms of rubrene and its derivatives, and this error can lead to serious problems when trying to understand rubrene behavior in the solid state. In cases like perfluororubrene, the functionals incorrectly suggest that the twisted structure is more stable, when it appears that the planar rubrene polymorph is actually preferred. This error is a manifestation of density-driven delocalization error which needs to be addressed in order to model these species correctly. These limitations can be overcome by using higher-level electronic structure methods like SCS-MP2D or DLPNO-CCSD(T). State-of-the-art double-hybrid density functionals[101,102] might also perform reasonably as well.

Although the twisting energy reductions of several kJ/mol (or $\sim$1–3 kT) observed here with the more accurate models may seem small from the perspective of solution-phase molecular dynamics, they could have an important impact on the prospects for conformational polymorphism in rubrene derivatives. Conformational polymorphs occur when adopting a strained intramolecular conformation is compensated for by the new favorable intermolecular interactions it enables. Crystal structures exhibiting smaller strain/conformational energy differences are considerably more probable than those that exhibit much larger differences. For example, a survey of 311 polymorph pairs with significant intramolecular conformational differences found that $\sim$50% had conformational energy differences less than 3.5 kJ/mol, $\sim$70% less than 5.5 kJ/mol, and $\sim$90% less than 14.5 kJ/mol.[23] Larger conformational energy differences are typically associated with specific circumstances, such as when switching from intra- to intermolecular hydrogen bonding[23] or when dramatically increasing the effective molecular surface area (e.g. changing from a folded to unfolded conformation).[84] Neither of those scenarios is applicable to rubrene. Moreover, a separate survey of 55 conformational polymorph pairs found that 74% had lattice energy differences of less than 6 kJ/mol, and 96% were below 10 kJ/mol.[22] Smaller intramolecular energy differences between conformations will be more readily compensated for through improved intermolecular interactions such that the overall energetics lie within these lattice energy windows.

All of these survey results speak toward relatively small conformational energy differences being an important precondition for the occurrence of conformational polymorphism. The fact that the rubrene twisting energies are found here to be several kJ/mol smaller than previously believed appreciably raises the likelihood of discovering conformational polymorphs of rubrene and its derivatives which differ in the tetracene backbone twisting. A number of previous studies have synthesized derivatives and tested to see whether they crystallize in planar or twisted forms. In many of those cases, however, relatively little effort was spent screening for alternative polymorphs. The results here suggest that it may be worthwhile to revisit some of those systems to search for planar crystal polymorphs of rubrene derivatives that have previously only been observed to crystallize in twisted conformations, in the hopes of finding improved crystal packing
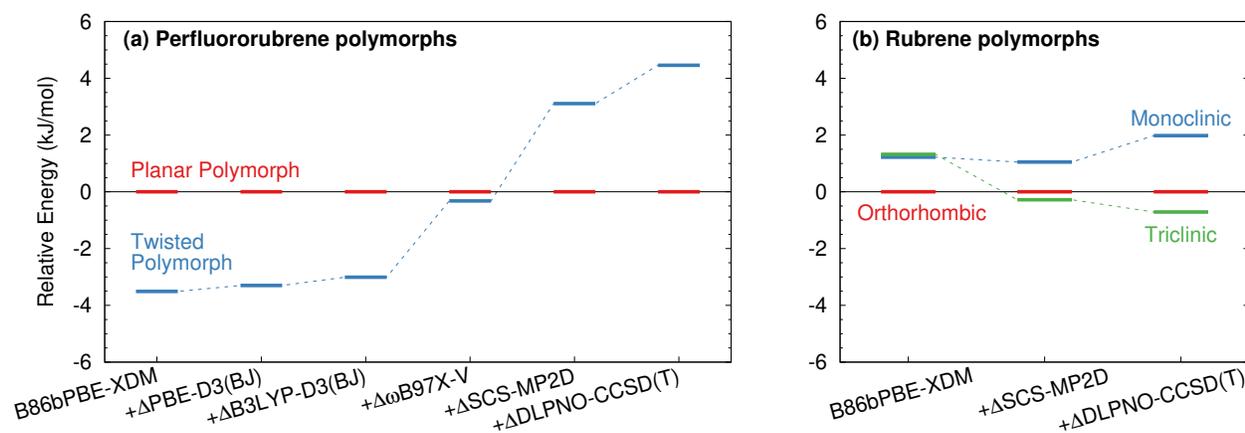
Fig. 5 Relative stabilities for the polymorphs of (a) perfluororubrene and (b) rubrene as computed with periodic B86bPBE-XDM and after correcting the monomer conformational energy with the method indicated ("Δ methods").

motifs for species that exhibit promising intrinsic electronic properties. Such experimental efforts could potentially be guided by crystal structure prediction studies that identify promising derivatives with a diversity of stable conformational polymorphs on the crystal energy landscape.

Conflicts of interest

There are no conflicts to declare.

Acknowledgements

Notes and references

1 J. Takeya, M. Yamagishi, Y. Tominari, R. Hirahara, Y. Nakazawa, T. Nishikawa, T. Kawase, T. Shimoda and S. Ogawa, *Appl. Phys. Lett.*, 2007, **90**, 102120.

2 G. Schweicher, G. Garbay, R. Jouclas, F. Vibert, F. Devaux and Y. H. Geerts, *Adv. Mater.*, 2020, **32**, 1905909.

3 M. Kytka, L. Gisslen, A. Gerlach, U. Heinemeyer, J. Kováč, R. Scholz and F. Schreiber, *J. Chem. Phys*, 2009, **130**, 214507.

4 J. L. Bredas, J. P. Calbert, D. A. da Silva Filho and J. Cornil, *Proc. Nat. Acad. Sci.*, 2002, **99**, 5804–5809.

5 D. A. Da Silva Filho, E. G. Kim and J. L. Brédas, *Advanced Materials*, 2005, **17**, 1072–1076.

6 M. L. Clapham, E. C. Murphy and C. J. Douglas, *Synthesis*, 2020, in press, DOI: 10.1055/s–0040–1707316.

7 D. Käfer, L. Ruppel, G. Witte and C. Wöll, *Phys. Rev. Lett.*, 2005, **95**, 166602.

8 S. Haas, A. Stassen, G. Schuck, K. Pernstich, D. Gundlach, B. Batlogg, U. Berens and H.-J. Kirner, *Phys. Rev. B*, 2007, **76**, 1–6.

9 A. S. Paraskar, A. R. Reddy, A. Patra, Y. H. Wijsboom, O. Gidron, L. J. W. Shimon, G. Leitus and M. Bendikov, *Chem. Eur. J.*, 2008, **14**, 10639–10647.

10 C. Sutton, M. S. Marshall, C. D. Sherrill, C. Risko and J.-L. Bredas, *J. Am. Chem. Soc.*, 2015, **137**, 8775–8782.

11 W. A. Ogden, S. Ghosh, M. J. Bruzek, K. A. McGarry, L. Balhorn, V. Young, L. J. Purvis, S. E. Wegwerth, Z. Zhang, N. A. Serratore, C. J. Cramer, L. Gagliardi and C. J. Douglas, *Cryst. Growth Des.*, 2017, **17**, 643–658.

12 O. D. Jurchescu, A. Meetsma and T. T. M. Palstra, *Acta Cryst. B*, 2006, **62**, 330–334.

13 L. Huang, Q. Liao, Q. Shi, H. Fu, J. Ma and J. Yao, *J. Mater. Chem.*, 2010, **20**, 159–166.

14 S. Bergantin and M. Moret, *Cryst. Growth Des.*, 2012, **12**, 6035–6041.

15 K. A. McGarry, W. Xie, C. Sutton, C. Risko, Y. Wu, V. G. Young, J.-L. Brédas, C. D. Frisbie and C. J. Douglas, *Chem. Mater.*, 2013, **25**, 2254–2263.

16 S. Uttiya, L. Miozzo, E. M. Fumagalli, S. Bergantin, R. Ruffo, M. Parravicini, A. Papagni, M. Moret and A. Sassella, *J. Mater. Chem. C*, 2014, **2**, 4147–4155.

17 M. Mamada, H. Katagiri, T. Sakanoue and S. Tokito, *Cryst. Growth Des.*, 2015, **15**, 442–448.

18 Y. Wu, X. Ren, K. A. McGarry, M. J. Bruzek, C. J. Douglas and C. D. Frisbie, *Adv. Elec. Mater.*, 2017, **3**, 1700117.

19 G. Xie, S. Hahn, F. Rominger, J. Freudenberg and U. H. F. Bunz, *Chem. Commun.*, 2018, **54**, 7593–7596.

20 Z. Zhang, W. A. Ogden, V. G. Young and C. J. Douglas, *Chem. Commun.*, 2016, **52**, 8127–8130.

21 Y. Sakamoto and T. Suzuki, *J. Org. Chem.*, 2017, **82**, 8111–8116.

22 A. J. Cruz-Cabeza, S. M. Reutzel-Edens and J. Bernstein, *Chem. Soc. Rev.*, 2015, **44**, 8619–8635.

23 A. J. Cruz-Cabeza and J. Bernstein, *Chem. Rev.*, 2014, **114**, 2170–2191.

24 J. Nyman and G. M. Day, *CrystEngComm*, 2015, **17**, 5154–5165.

25 S. L. Price, *Chem. Soc. Rev.*, 2014, **43**, 2098–111.

26 S. L. Price, D. E. Braun and S. M. Reutzel-Edens, *Chem. Com-*

mun., 2016, **52**, 7065–7077.

27 G. M. Day, T. G. Cooper, A. J. Cruz-Cabeza, K. E. Hejczyk, H. L. Ammon, S. X. M. Boerrigter, J. S. Tan, R. G. Della Valle, E. Venuti, J. Jose, S. R. Gadre, G. R. Desiraju, T. S. Thakur, B. P. van Eijck, J. C. Facelli, V. E. Bazterra, M. B. Ferraro, D. W. M. Hofmann, M. A. Neumann, F. J. J. Leusen, J. Kendrick, S. L. Price, A. J. Misquitta, P. G. Karamertzanis, G. W. A. Welch, H. A. Scheraga, Y. A. Arnautova, M. U. Schmidt, J. van de Streek, A. K. Wolf and B. Schweizer, *Acta Cryst. B*, 2009, **65**, 107–125.

28 D. A. Bardwell, C. S. Adjiman, Y. A. Arnautova, E. Bartashevich, S. X. M. Boerrigter, D. E. Braun, A. J. Cruz-Cabeza, G. M. Day, R. G. Della Valle, G. R. Desiraju, B. P. van Eijck, J. C. Facelli, M. B. Ferraro, D. Grillo, M. Habgood, D. W. M. Hofmann, F. Hofmann, K. V. J. Jose, P. G. Karamertzanis, A. V. Kazantsev, J. Kendrick, L. N. Kuleshova, F. J. J. Leusen, A. V. Maleev, A. J. Misquitta, S. Mohamed, R. J. Needs, M. A. Neumann, D. Nikylov, A. M. Orendt, R. Pal, C. C. Pantelides, C. J. Pickard, L. S. Price, S. L. Price, H. A. Scheraga, J. van de Streek, T. S. Thakur, S. Tiwari, E. Venuti and I. K. Zhitkov, *Acta Cryst. B*, 2011, **67**, 535–551.

29 A. M. Reilly, R. I. Cooper, C. S. Adjiman, S. Bhattacharya, A. D. Boese, J. G. Brandenburg, P. J. Bygrave, R. Bylsma, J. E. Campbell, R. Car, D. H. Case, R. Chadha, J. C. Cole, K. Cosburn, H. M. Cuppen, F. Curtis, G. M. Day, R. A. DiStasio Jr, A. Dzyabchenko, B. P. van Eijck, D. M. Elking, J. A. van den Ende, J. C. Facelli, M. B. Ferraro, L. Fusti-Molnar, C.-A. Gatsiou, T. S. Gee, R. de Gelder, L. M. Ghiringhelli, H. Goto, S. Grimme, R. Guo, D. W. M. Hofmann, J. Hoja, R. K. Hylton, L. Iuzzolino, W. Jankiewicz, D. T. de Jong, J. Kendrick, N. J. J. de Klerk, H.-Y. Ko, L. N. Kuleshova, X. Li, S. Lohani, F. J. J. Leusen, A. M. Lund, J. Lv, Y. Ma, N. Marom, A. E. Masunov, P. McCabe, D. P. McMahon, H. Meekes, M. P. Metz, A. J. Misquitta, S. Mohamed, B. Monserrat, R. J. Needs, M. A. Neumann, J. Nyman, S. Obata, H. Oberhofer, A. R. Oganov, A. M. Orendt, G. I. Pagola, C. C. Pantelides, C. J. Pickard, R. Podeszwa, L. S. Price, S. L. Price, A. Pulido, M. G. Read, K. Reuter, E. Schneider, C. Schober, G. P. Shields, P. Singh, I. J. Sugden, K. Szalewicz, C. R. Taylor, A. Tkatchenko, M. E. Tuckerman, F. Vacarro, M. Vasileiadis, A. Vazquez-Mayagoitia, L. Vogt, Y. Wang, R. E. Watson, G. A. de Wijs, J. Yang, Q. Zhu and C. R. Groom, *Acta Cryst. B*, 2016, **72**, 439–459.

30 M. A. Neumann, J. van de Streek, F. P. A. Fabbiani, P. Hidber and O. Grassmann, *Nature Commun.*, 2015, **6**, 7793.

31 A. Pulido, L. Chen, T. Kaczorowski, D. Holden, M. A. Little, S. Y. Chong, B. J. Slater, D. P. McMahon, B. Bonillo, C. J. Stackhouse, A. Stephenson, C. M. Kane, R. Clowes, T. Hasell, A. I. Cooper and G. M. Day, *Nature*, 2017, **543**, 657–664.

32 J. Yang, C. T. Hu, X. Zhu, Q. Zhu, M. D. Ward and B. Kahr, *Angew. Chem. Int. Ed.*, 2017, **56**, 10165–10169.

33 R. M. Bhardwaj, J. A. McMahon, J. Nyman, L. S. Price, S. Konar, I. D. H. Oswald, C. R. Pulham, S. L. Price and S. M. Reutzel-Edens, *J. Am. Chem. Soc.*, 2019, **141**, 13887–13897.

34 J. Hoja, H.-Y. Ko, M. A. Neumann, R. Car, R. A. DiStasio and

A. Tkatchenko, *Science Adv.*, 2019, **5**, eaau3338.

35 M. Mortazavi, J. Hoja, L. Aerts, L. Quéré, J. van de Streek, M. A. Neumann and A. Tkatchenko, *Commun. Chem.*, 2019, **2**, 80.

36 X. Li, X. Ou, H. Rong, S. Huang, J. Nyman, L. Yu and M. Lu, *Cryst. Growth Des.*, 2020, acs.cgd.0c01017.

37 S. L. Price and S. M. Reutzel-Edens, *Drug Disc. Today*, 2016, **21**, 912–923.

38 A. N. Sokolov, S. Atahan-Evrenk, R. Mondal, H. B. Akkerman, R. S. Sánchez-Carrera, S. Granados-Focil, J. Schrier, S. C. Mannsfeld, A. P. Zoombelt, Z. Bao and A. Aspuru-Guzik, *Nature Commun.*, 2011, **2**, 437.

39 J. Yang, S. De, J. E. Campbell, S. Li, M. Ceriotti and G. M. Day, *Chem. Mater.*, 2018, **30**, 4361–4371.

40 C. Y. Cheng, J. E. Campbell and G. M. Day, *Chem. Sci.*, 2020, **11**, 4922–4933.

41 V. Coropceanu, J. Cornil, D. A. da Silva Filho, Y. Olivier, R. Silbey and J.-L. Brédas, *Chem. Rev.*, 2007, **107**, 926–952.

42 C. Sutton, C. Risko and J.-L. Brédas, *Chem. Mater.*, 2016, **28**, 3–16.

43 X. Wang, T. Garcia, S. Monaco, B. Schatschneider and N. Marom, *CrystEngComm*, 2016, **18**, 7353–7362.

44 S. Grimme, A. Hansen, J. G. Brandenburg and C. Bannwarth, *Chem. Rev.*, 2016, **116**, 5105–5154.

45 J. Hermann, R. A. DiStasio and A. Tkatchenko, *Chem. Rev.*, 2017, **117**, 4714–4758.

46 A. J. Cohen, P. Mori-Sanchez and W. Yang, *Science*, 2008, **321**, 792–794.

47 A. J. Cohen, P. Mori-Sanchez and W. Yang, *Chem. Rev.*, 2012, **112**, 289–320.

48 L. M. LeBlanc, S. G. Dale, C. R. Taylor, A. D. Becke, G. M. Day and E. R. Johnson, *Angew. Chem. Int. Ed.*, 2018, **57**, 14906–14910.

49 B. G. Johnson, C. A. Gonzales, P. M. Gill and J. A. Pople, *Chem. Phys. Lett.*, 1994, **221**, 100–108.

50 O. V. Gritsenko, B. Ensing, P. R. T. Schipper and E. J. Baerends, *J. Phys. Chem. A*, 2000, **104**, 8558–8565.

51 S. Patchkovskii and T. Ziegler, *J. Chem. Phys.*, 2002, **116**, 7806–7813.

52 S. Andersson and M. Grüning, *J. Phys. Chem. A*, 2004, **108**, 7621–7636.

53 T. Bally and G. N. Sastry, *J. Phys. Chem. A*, 1997, **101**, 7923–7925.

54 A. Ruzsinszky, J. P. Perdew, G. I. Csonka, O. A. Vydrov and G. E. Scuseria, *J. Chem. Phys.*, 2006, **125**, 194112.

55 A. D. Dutoi and M. Head-Gordon, *Chem. Phys. Lett.*, 2006, **422**, 230–233.

56 H. L. Woodcock, H. F. Schaefer and P. R. Schreiner, *J. Phys. Chem. A*, 2002, **106**, 11923–11931.

57 E. R. Johnson, P. Mori-Sánchez, A. J. Cohen and W. Yang, *J. Chem. Phys.*, 2008, **129**, 204112.

58 T. Heaton-Burgess and W. Yang, *J. Chem. Phys.*, 2010, **132**, 234113.

59 C. Greenwell, J. L. McKinley, P. Zhang, Q. Zeng, G. Sun, B. Li,

S. Wen and G. J. O. Beran, *Chem. Sci.*, 2020, **11**, 2200–2214.

60 C. Greenwell and G. J. O. Beran, *Cryst. Growth Des.*, 2020, **20**, 4875–4881.

61 M.-C. Kim, E. Sim and K. Burke, *Phys. Rev. Lett.*, 2013, **111**, 073003.

62 B. G. Janesko and G. E. Scuseria, *J. Chem. Phys.*, 2008, **128**, 244112.

63 P. Verma, A. Perera and R. J. Bartlett, *Chem. Phys. Lett.*, 2012, **524**, 10–15.

64 M.-C. Kim, E. Sim and K. Burke, *J. Chem. Phys.*, 2014, **140**, 18A528.

65 M.-C. Kim, H. Park, S. Son, E. Sim and K. Burke, *J. Phys. Chem. Lett.*, 2015, **6**, 3802–3807.

66 J. Řezáč, C. Greenwell and G. J. O. Beran, *J. Chem. Theory Comput.*, 2018, **14**, 4711–4721.

67 C. Greenwell, J. Řezáč and G. J. O. Beran, *submitted*, 2021.

68 S. Grimme, L. Goerigk and R. F. Fink, *WIRES: Comput. Mol. Sci.*, 2012, **2**, 886–906.

69 S. Grimme, *J. Chem. Phys.*, 2003, **118**, 9095.

70 R. A. DiStasio and M. Head-Gordon, *Mol. Phys.*, 2007, **105**, 1073–1083.

71 J. G. Hill and J. A. Platts, *J. Chem. Theory Comput.*, 2007, **3**, 80–85.

72 R. A. King, *Molecular Physics*, 2009, **107**, 789–795.

73 J. Rigby and E. I. Izgorodina, *J. Chem. Theory Comput.*, 2014, **10**, 3111–3122.

74 S. Tan, S. Barrera Acevedo and E. I. Izgorodina, *J. Chem. Phys.*, 2017, **146**, 064108.

75 R. T. McGibbon, A. G. Taube, A. G. Donchev, K. Siva, F. Hernández, C. Hargus, K.-H. Law, J. L. Klepeis and D. E. Shaw, *J. Chem. Phys.*, 2017, **147**, 161725.

76 I. Cacelli, F. Lipparini, L. Greff da Silveira, M. Jacobs, P. R. Livotto and G. Prampolini, *The Journal of Chemical Physics*, 2019, **150**, 234113.

77 S. M. Cybulski and M. L. Lytle, *J. Chem. Phys.*, 2007, **127**, 141102.

78 A. Hesselmann, *J. Chem. Phys.*, 2008, **128**, 144112.

79 M. Pitonak and A. Hesselmann, *J. Chem. Theory Comput.*, 2010, **6**, 168–178.

80 A. Tkatchenko, R. A. DiStasio, M. Head-Gordon and M. Scheffler, *J. Chem. Phys.*, 2009, **131**, 094106.

81 Y. Huang, M. Goldey, M. Head-Gordon and G. J. O. Beran, *J. Chem. Theory Comput.*, 2014, **10**, 2054–2063.

82 G. J. O. Beran, *CrystEngComm*, 2019, **21**, 758–764.

83 D. Casanova, *J. Chem. Theory Comput.*, 2014, **10**, 324–334.

84 H. P. G. Thompson and G. M. Day, *Chem. Sci.*, 2014, **5**, 3173–3182.

85 M. J. Frisch, G. W. Trucks, H. B. Schlegel, G. E. Scuseria, M. A. Robb, J. R. Cheeseman, G. Scalmani, V. Barone, B. Mennucci, G. A. Petersson, H. Nakatsuji, M. Caricato, X. Li, H. P. Hratchian, A. F. Izmaylov, J. Bloino, G. Zheng, J. L. Sonnenberg, M. Hada, M. Ehara, K. Toyota, R. Fukuda, J. Hasegawa, M. Ishida, T. Nakajima, Y. Honda, O. Kitao, H. Nakai, T. Vreven, J. A. Montgomery, Jr., J. E. Peralta, F. Ogliaro, M. Bearpark, J. J. Heyd, E. Brothers, K. N. Kudin, V. N. Staroverov, R. Kobayashi, J. Normand, K. Raghavachari, A. Rendell, J. C. Burant, S. S. Iyengar, J. Tomasi, M. Cossi, N. Rega, J. M. Millam, M. Klene, J. E. Knox, J. B. Cross, V. Bakken, C. Adamo, J. Jaramillo, R. Gomperts, R. E. Stratmann, O. Yazyev, A. J. Austin, R. Cammi, C. Pomelli, J. W. Ochterski, R. L. Martin, K. Morokuma, V. G. Zakrzewski, G. A. Voth, P. Salvador, J. J. Dannenberg, S. Dapprich, A. D. Daniels, Ö. Farkas, J. B. Foresman, J. V. Ortiz, J. Cioslowski and D. J. Fox, *Gaussian 09 Revision E.01*, 2009, Gaussian Inc. Wallingford CT.

86 R. M. Parrish, L. A. Burns, D. G. A. Smith, A. C. Simmonett, A. E. DePrince, E. G. Hohenstein, U. Bozkaya, A. Y. Sokolov, R. Di Remigio, R. M. Richard, J. F. Gonthier, A. M. James, H. R. McAlexander, A. Kumar, M. Saitow, X. Wang, B. P. Pritchard, P. Verma, H. F. Schaefer, K. Patkowski, R. A. King, E. F. Valeev, F. A. Evangelista, J. M. Turney, T. D. Crawford and C. D. Sherrill, *J. Chem. Theory Comput.*, 2017, **13**, 3185–3197.

87 F. Weigend and R. Ahlrichs, *Phys. Chem. Chem. Phys.*, 2005, **7**, 3297–3305.

88 T. Helgaker, W. Klopper, H. Koch and J. Noga, *J. Chem. Phys.*, 1997, **106**, 9639–9646.

89 T. H. Dunning, *J. Chem. Phys.*, 1989, **90**, 1007–1023.

90 C. Riplinger, B. Sandhoefer, A. Hansen and F. Neese, *J. Chem. Phys.*, 2013, **139**, 134101.

91 F. Neese, *WIREs Comput. Molec. Sci.*, 2012, **2**, 73–78.

92 A. G. Császár, W. D. Allen and H. F. Schaefer, *J. Chem. Phys.*, 1998, **108**, 9751–9764.

93 P. Giannozzi, O. Andreussi, T. Brumme, O. Bunau, M. Buongiorno Nardelli, M. Calandra, R. Car, C. Cavazzoni, D. Ceresoli, M. Cococcioni, N. Colonna, I. Carnimeo, A. Dal Corso, S. de Gironcoli, P. Delugas, R. A. DiStasio, A. Ferretti, A. Floris, G. Fratesi, G. Fugallo, R. Gebauer, U. Gerstmann, F. Giustino, T. Gorni, J. Jia, M. Kawamura, H.-Y. Ko, A. Kokalj, E. Küçükbenli, M. Lazzeri, M. Marsili, N. Marzari, F. Mauri, N. L. Nguyen, H.-V. Nguyen, A. Otero-de-la Roza, L. Paulatto, S. Poncé, D. Rocca, R. Sabatini, B. Santra, M. Schlipf, A. P. Seitsonen, A. Smogunov, I. Timrov, T. Thonhauser, P. Umari, N. Vast, X. Wu and S. Baroni, *J. Phys. Condens. Mat.*, 2017, **29**, 465901.

94 J. A. Chisholm and W. D. S. Motherwell, *J. Appl. Crystall.*, 2005, **38**, 228–231.

95 S. R. Whittleton, A. Otero-de-la Roza and E. R. Johnson, *J. Chem. Theory Comput.*, 2017, **13**, 5332–5342.

96 S. L. Price, *Faraday Disc.*, 2018, **211**, 9–30.

97 A. M. Reilly and A. Tkatchenko, *Phys. Rev. Lett.*, 2014, **113**, 055701.

98 S. R. Whittleton, A. Otero-de-la Roza and E. R. Johnson, *J. Chem. Theory Comput.*, 2017, **13**, 441–450.

99 M. Yang, E. Dybeck, G. Sun, C. Peng, B. Samas, V. M. Burger, Q. Zeng, Y. Jin, M. A. Bellucci, Y. Liu, P. Zhang, J. Ma, Y. A. Jiang, B. C. Hancock, S. Wen and G. P. F. Wood, *Cryst. Growth Des.*, 2020, **20**, 5211–5224.

100 N. P. Schieber, E. C. Dybeck and M. R. Shirts, *J. Chem. Phys.*, 2018, **148**, 144104.

101 N. Mardirossian and M. Head-Gordon, *J. Chem. Phys.*, 2018, **148**, 241736.

102 G. Santra, N. Sylvetsky and J. M. L. Martin, *J. Phys. Chem. A*, 2019, **123**, 5129–5143.